Unravelling the effects of calcium substitution in $BaGd_2CoO_5$ Haldane gap 1D material and its thermoelectric performance

Narendar Nasani[1,2]*, Andrei V. Kovalevsky[3], Wenjie Xie[4], Shahed Rasekh[3], Gabriel Constantinescu[3], Anke Weidenkaff[4], D. Pukazhselvan[2] and Duncan P. Fagg[2]

[1]Centre for Materials for Electronics Technology (C-MET), (Under Ministry of Electronics & Information Technology (MeitY), Govt. of India), Panchawati, Pune, 411-008, India.

[2]Centre for Mechanical Technology and Automation (TEMA), Department of Mechanical Engineering, University of Aveiro, 3810-193, Aveiro, Portugal.

[3]Department of Materials and Ceramic Engineering, CICECO, University of Aveiro, 3810-193 Aveiro, Portugal.

[4]Materials and Resources, Technical University of Darmstadt, Alarich-Weiss Str.2, DE-64287 Darmstadt, Germany.

* Corresponding author email: narendar.nasani@cmet.gov.in;

Tel. No. +91(020) 25898724

Abstract

Eco-benign and high-temperature-stable oxides are considered a promising alternative to traditional Bi_2Te_3, Bi_2Se_3 and PbTe-based thermoelectric materials. The quest for high performing thermoelectric oxides is still open and, among other challenges, includes the screening of various materials systems for potentially promising electrical and thermal transport properties. In this work, a new family of acceptor-substituted Haldane gap 1D $BaGd_2CoO_5$ dense ceramic materials was characterized in this respect. The substitution of this material with calcium results in a general improvement of the electrical performance, contributed by an interplay between the charge carrier concentration and their mobility. Nevertheless, a relatively low electrical conductivity was measured, reaching ~5 S/cm at 1175 K, resulting in a maximum power factor of ~25 $\mu W/(K \times m^2)$ at 1173 K, for $BaGd_{1.80}Ca_{0.20}CoO_5$. On the other hand, the unique anisotropic 1D structure of the prepared materials promotes efficient phonon scattering, leading to low thermal conductivities, rarely observed in oxide electroceramics. While the $BaGd_{2-x}Ca_xCoO_5$ materials show attractive Seebeck coefficient values in the range 210-440 $\mu V/K$, the resulting dimensionless figure of merit is still relatively low, reaching ~0.02 at 1173 K. The substituted $BaGd_{2-x}Ca_xCoO_5$ ceramics show comparable thermoelectric performance in both inert and air atmospheres. These features highlight the potential relevance of this structure type for thermoelectric application, with future emphasis placed on methods to improve conductivity.

Keywords: Haldane gap; thermal conductivity; thermoelectrics; seebeck coefficient; figure of merit

1. Introduction

In recent years, the rapid depletion of fossil fuel resources and subsequent potential future oil crises, together with environmental-related problems, have led the researchers to focus their work more on alternative energy conversion and storage devices such as batteries, fuel cells, solar cells, supercapacitors and solar thermoelectric generators[1–3] to meet the increased energy demand. Among them, solar thermoelectric generation offers the unique possibility to directly convert solar heat into electrical power, based on the Seebeck effect[4–6]. These solid-state devices are robust, reliable and scalable, have no moving parts and do not require maintenance. Despite these advantages, the performance and efficiency of thermoelectric devices is rather low and is limited by several factors, their use being reserved mainly for niche applications, where their advantages outweigh their disadvantages[7,8]. Furthermore, the search for environmentally benign, highly abundant and non-toxic materials is in prime focus for these devices, if targeting a reasonable range of potential applications. To this end, oxide-based thermoelectric materials have been introduced as promising alternatives to the state-of-the-art 'traditional' critical lead, antimony, bismuth, tellurium and selenium-containing thermoelectric intermetallic alloys, due to their ability to work in the air at high temperatures, without degradation or decomposition[6,8].

The thermoelectric performance is usually given by the dimensionless figure of merit, $ZT = \frac{S^2 \sigma T}{k}$, where S is the Seebeck coefficient or thermopower, σ is the electrical conductivity, T is the absolute temperature and κ is the total thermal conductivity[6,8–10]. High Seebeck coefficient and electrical conductivity, simultaneously with low thermal conductivity, are essential requirements in achieving high ZT values at any given temperature. However, all these parameters are not independent of each-other, meaning that enhancing the charge carrier concentration, for example, a strategy usually pursued

in this type of functional materials, must not be performed at the expense of increasing the thermal conductivity[10–12]. Although oxide thermoelectrics show excellent thermal and chemical stability in air at high temperatures, their known performance is still not comparable to that of established thermoelectric materials, in the relevant working-temperature range. This is mainly due to the relatively low charge carrier mobility values, provided mainly by the ionic bonding and the high thermal conductivity values, characteristic for oxide materials.

The most widely studied oxide materials for thermoelectric generation are the n-type ZnO, $SrTiO_3$, $CaMnO_3$ and In_2O_3, and the p-type $Ca_3Co_4O_9$, $NaCo_2O_4$, BiCuSeO and NiO[8,10,11,13–21]. Their performance is further enhanced by aliovalent metal doping, defect engineering and nanostructuring[9,22]. In the pursuit of new materials, Mandvi et al. studied the double perovskite oxide material $(Ba,Sr)_2TiMoO_6$ for thermoelectric applications and found the electrical conductivity values between 10^4-10^5 S/cm in the temperature range 300-1223 K[23]. On the other hand, the Seebeck coefficient and thermal conductivity (5.8 W/mK at 1150 K) values of this material are yet to be improved. The thermoelectric performance of stoichiometric and non- stoichiometric donor-substituted strontium titanates has been widely studied and achieved the dimensionless figure of merit of 0.35-0.40 at 1200 K[10,14,21,22,24–26]. Layered $Ca_3Co_4O_9$-based materials have also attracted huge attention as promising p-type thermoelectrics, reaching *ZT* of 0.3-0.7 at 1000 K[17,27,28].

In the quest for new oxide materials, our team has systematically studied for the first time the thermoelectric performance of one dimensional (1D) $BaGd_2NiO_5$ Haldane gap material [12]. The ubiquitous 1D structure, low thermal conductivity and impressive Seebeck coefficient values of Haldane gap materials have convinced us to explore a similar family of cobalt-rich materials i.e. $BaGd_2CoO_5$, for thermoelectric applications.

The cobaltite-based materials were identified to be highly stable at high temperatures, eco-friendly and widely available in nature[16–18,29]. The stability of BaR_2CoO_5 (R = rare earth) materials has been explained based on the global instability index (GII) using a bond valence method, and it was found that the rare-earth-based oxides possess a very high internal stress value of 0.2 v.u.[30] The main structural feature of these materials is the existence of a one-dimensional arrangement of vertex-sharing (CoO_6) flattened octahedra, successively parallel to the crystallographic a-axis[31]. These octahedral chains are intertwined with monocapped (RO_7) trigonal prisms, while the barium cations are closely surrounded by ten oxygen atoms, forming bicapped (BaO_{10}) square prisms. The very short distance between Co-O-Co atoms is shown to have a profound effect on the behavior of Co^{2+} sublattice and is responsible for the typical 1D antiferromagnetic behavior of these materials[30,31].

The current work assesses the impact of acceptor doping in $BaGd_2CoO_5$ Haldane gap material on the structural, microstructural, electrical and thermal properties. The thermoelectric performance of novel $BaGd_{2-x}Ca_xCoO_5$ (x=0.00-0.30) materials is evaluated in the temperature range 400−1173 K, under air and argon atmospheres.

2. Experimental

All $BaGd_{2-x}Ca_xCoO_5$ (x=0.00-0.30) Haldane gap ceramics were synthesized by solid-state reaction method using reagent grade BaO_2 (Sigma Aldrich), $CaCO_3$ (Sigma Aldrich), Gd_2O_3 (Sigma Aldrich) and Co_3O_4 (Sigma Aldrich) precursor powders as starting materials. Before weighing, the Gd_2O_3 powder was heated to 1223 K (2 h dwell time) and cooled down to 523 K, to remove any absorbed moisture. The stoichiometric amounts of precursor materials were weighed and mixed in absolute ethanol (Sigma Aldrich), using an agate mortar and pestle, until a homogeneous mixture was obtained,

followed by drying at 353 K. The dried powders were uniaxially pressed in disc-shaped samples and fired at 1273 K and 1373 K for 15 h in flowing argon, with an intermediate grinding step. The resulted sintered pellets were crushed into powders and uniaxially pressed again into disc-shaped samples. These final green pellets were sintered at 1553 K for 6 h in a controlled argon atmosphere, for further structural, microstructural, electrical and thermal characterizations.

The density of sintered pellets (ρ_{exp}), determined by geometrical measurements and weighing, was found to be ≥90% of the theoretical density (ρ_{th}), calculated from the structural data. The studied $BaGd_{2-x}Ca_xCoO_5$ compositions are also denoted as BGCC00, BGCC05, BGCC10, BGCC15 etc., for x=0.00, 0.05, 0.10, 0.15 etc., respectively, for clarity.

The phase analysis was performed by powder X-ray diffraction (XRD) using a Philips X'Pert diffractometer equipped with an X'Celerator detector, with CuKα radiation, in the scan range 2Θ=20º-80º and with a step size of 0.02º and an exposure time of 30 s. The unit cell parameters and lattice volume were calculated using the Rietveld refinement method, with the Fullprof program [32]. The microstructural studies of fractured ceramics were conducted by scanning electron microscopy (SEM) (Hitachi SU-70), coupled with an energy dispersive X-ray spectroscopy (EDS) (Bruker Quantax 400 Germany), for elemental analyses.

In $BaGd_2CoO_5$ Haldane gap materials, the issues related to the oxygen nonstoichiometry and oxidation states of the transition metal cation represent an interesting topic for research [33]. To determine the oxygen content in the studied compositions, thermogravimetric analysis (TGA) was performed on powdered samples, at 600 and 1200 K. The relative weight change was monitored as a function of

temperature in flowing argon, followed by a complete reduction of cobalt in 10%H_2/N_2 gas mixture, at 1223 K for 2 h. The weight of the resulting mixture of oxides and metallic cobalt was then used as a reference in calculating the oxidation states of the cobalt cations from the ceramic samples.

The electrical conductivity and Seebeck coefficient values were simultaneously measured on bar-shaped samples (~1.3×0.3×0.4 cm) cut from sintered ceramic pellets, as described in previous works [1234]. All measurements were performed under both air and argon atmospheres, in the temperature range 400−1273 K, on cooling and using temperature steps between 50−80 K. An equilibrium criterion of less than 0.1% min^{-1} for electrical conductivity and less than 0.002 mV K^{-1} min^{-1} for Seebeck coefficient was used for relaxation rates after the temperature changes. The estimated experimental error in measured values did not exceed 3–5% for electrical conductivity and 5–7% for the Seebeck coefficient [35].

The thermal diffusivity (D) and specific heat capacity (C_p) studies were conducted with the standard Netzsch LFA 457 Microflash and Netzsch DSC 404F1 instruments, in both flowing air and argon atmospheres, using a measurement procedure identical to that used for the electrical measurements. The total thermal conductivity (κ) was calculated as $\kappa = D \times \rho \times C_p$. The estimated error of the obtained thermal conductivity values was less than 10% [35].The lattice thermal conductivity (κ_{ph}) was then evaluated from the well-known Wiedemann-Franz law as:

$$\kappa_{ph} = \kappa - \sigma L T \qquad (1)$$

where L (=$2.45 \cdot 10^{-8}$ W Ω K^{-2}) is the Sommerfeld value of the Lorenz number [36].

3. Results and Discussion

3.1. Structural characterization and microstructural evolution

As it was mentioned earlier, all $BaGd_{2-x}Ca_xCoO_5$ (x=0.00-0.30) Haldane gap ceramics were synthesized in an inert atmosphere, since the desired phase is not formed in air due to the oxidation of Co(II) to Co(III) [30]. The XRD patterns for all samples calcined at 1553 K in argon atmosphere are depicted in Fig. 1.

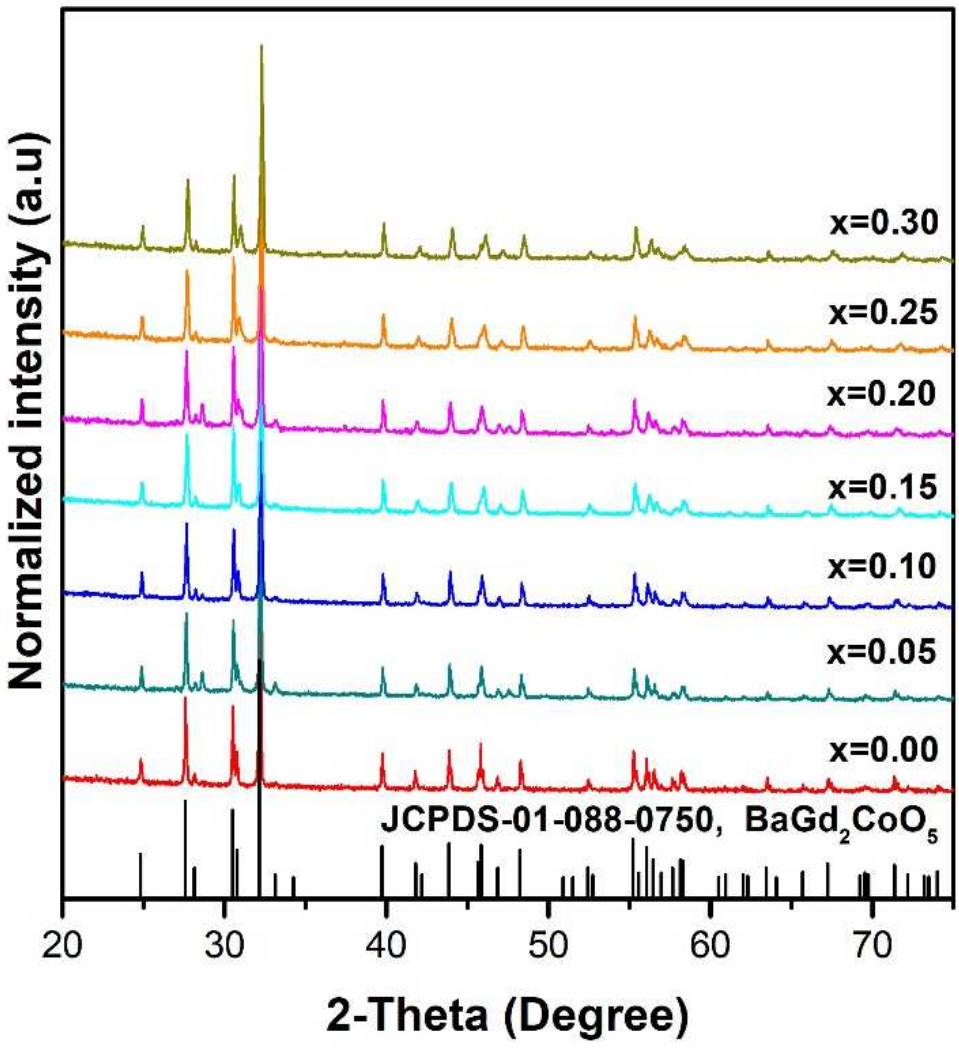

Figure 1. Powder XRD patterns of $BaGd_{2-x}Ca_xCoO_5$ (x=0.00-0.30) samples.

All the samples exhibit apparently single-phase composition, without any secondary peaks visible on the XRD patterns. The identified $BaGd_2CoO_5$ Haldane gap phase

belongs to an orthorhombic system (*Sp. gp*: *Imma)* and its refined lattice parameters and lattice volumes are presented in Table 1 and Fig. 2, as a function of Ca content.

Table 1. Lattice parameters of $BaGd_{2-x}Ca_xCoO_5$ (x=0.00-0.30) samples, obtained from Rietveld refinement.

%mol. Ca	Lattice parameters (Å)			V (Å^3)
	A	*B*	*C*	
0	3.76561	5.85477	11.62248	256.240
5	3.76413	5.85496	11.61472	255.970
10	3.76078	5.85319	11.60224	255.395
15	3.7586	5.85335	11.59301	255.051
20	3.75974	5.85336	11.592145	255.110
25	3.75686	5.85115	11.57607	254.435
30	3.75351	5.84849	11.55197	253.593

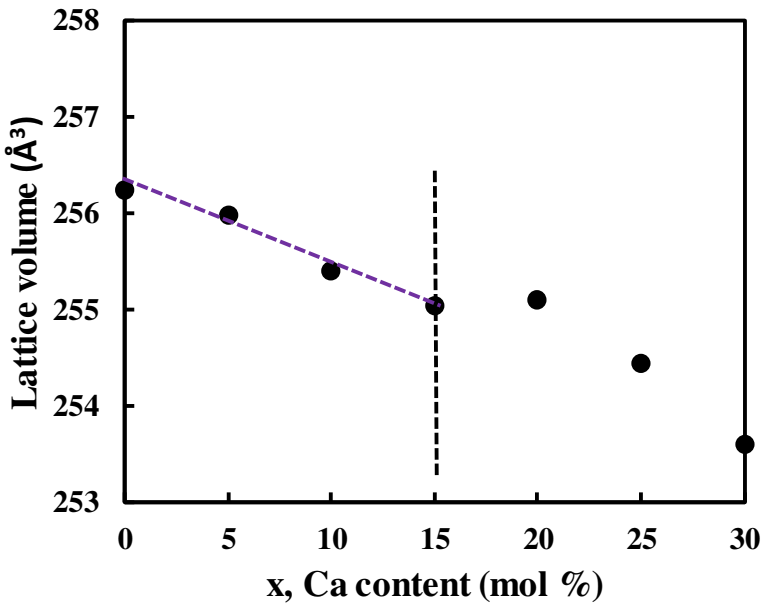

Figure 2. Variation of the unit cell volume with the Ca content in $BaGd_{2-x}Ca_xCoO_5$ samples.

Although the ionic size of Ca^{2+} (0.99 Å) is slightly larger than that of Gd^{3+} (0.93 Å), the lattice volume decreases continuously up to x=0.15, followed by a marginal increase at x=0.20 and another continuous decrease with a different slope (Fig. 2). This tendency indicates that the solid solution limit for the $BaGd_{2-x}Ca_xCoO_5$ materials occurs at

x=0.15. Similar tendencies were previously observed for other acceptor (Ca, Sr) doped Haldane gap analogue materials, e.g. $Ca_xBaGd_{2-x}NiO_5$ by Nasani et al.[12], $Y_{2-x}Ca_xBaNiO_5$ by Lannuzel et al.[37] and $Y_{2-x}Sr_xBaNiO_5$. by Nasani et al[38]. This behavior can be attributed to the growing contribution of charge compensation mechanisms on substitution, together with other additional factors, discussed below.

The SEM studies (Fig. 3) performed on selected fractured samples reveal high-quality ceramic materials having high density and small porosity.

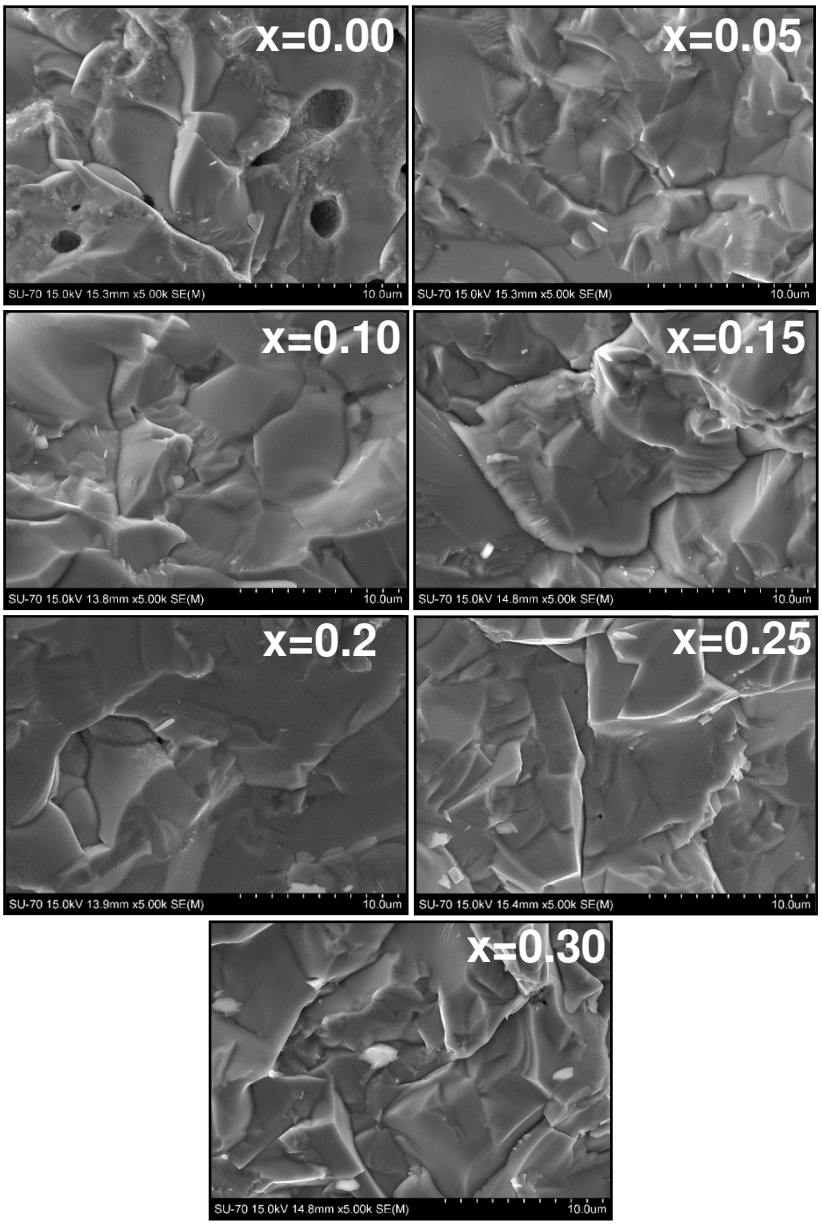

Figure 3. Selected SEM micrographs of fractured $BaGd_{2-x}Ca_xCoO_5$ (x=0.00-0.30) samples.

The representative SEM micrographs clearly show that all samples present a similar microstructure, represented by tightly-packed irregular grains of various shapes and sizes. The corresponding densities in each case are listed in Table 2.

Table 2. Calculated densities for $BaGd_{2-x}Ca_xCoO_5$ (x=0.00-0.30) samples.

Sample	ρ_{exp}/ρ_{th} (%)
BGCC0	89
BGCC5	92
BGCC10	93
BGCC15	93
BGCC20	91
BGCC25	88
BGCC30	87

At moderate concentration up to x=0.15, the presence of calcium improves the density of corresponding ceramics, while further substitution results in the appearance of residual porosity. More guidelines on these effects can be obtained from the representative results of EDS studies, shown in Fig. 4.

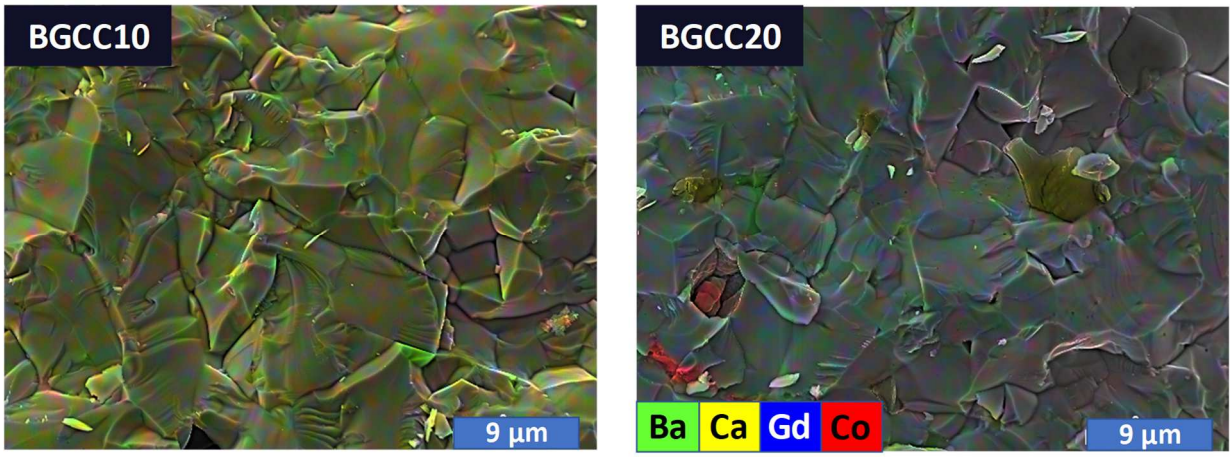

Figure 4. Selected EDS maps of fractured BGCC10 and BGCC20 samples.

The BGCC10 composition lies within the solid solution range and shows a homogeneous distribution of the constituent cations, in agreement with the XRD results (Fig. 1). On the other hand, the chemical mapping results for BGCC20 suggest the presence of local Ca- and Co-rich impurities, which were previously not detected by XRD, probably due to their small amounts. This fact is apparently responsible for the inflection observed on the unit cell volume *vs.* composition curves (Fig. 2), at x ≥0.15. The appearance of such impurities also correlates well with the decrease in relative density observed for x=0.20-0.30 (Table 2). This decrease might be also due to the volatilization of calcium at the high sintering temperature used in this work (1553 K).

Although the deviations from a single-phase composition may affect the interpretation of the TGA results, the observed tendencies shown in Fig. 5 are well-in-line with those expected for acceptor-type substitutions in $BaGd_{2-x}Ca_xCoO_5$ samples, at least for moderate calcium contents.

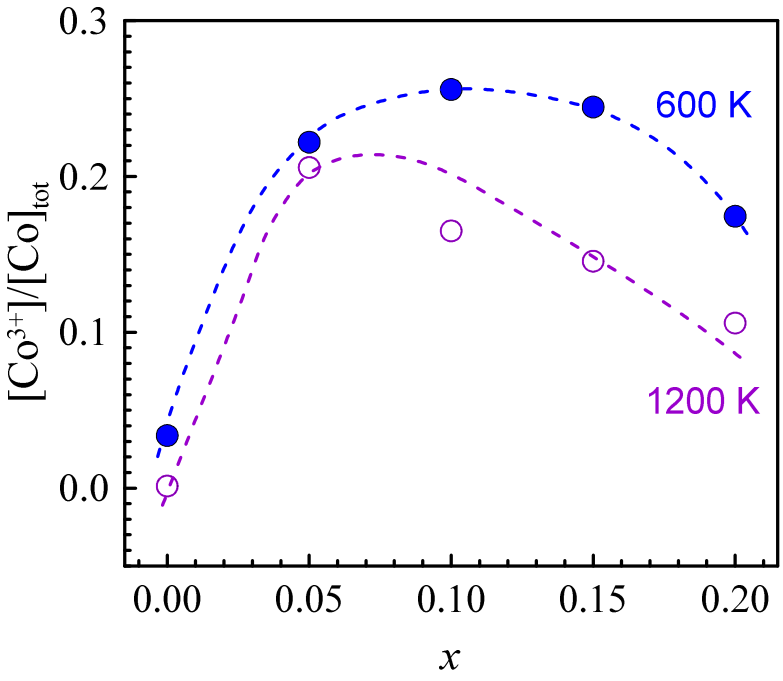

Figure 5. The effect of the nominal chemical composition of $BaGd_{2-x}Ca_xCoO_5$ samples on the fraction of Co^{3+} cations at 600 and 1200 K, in the solid solution range and for x=0.20, determined from the TGA studies.

As compared to the $Ca_xBaGd_{2-x}NiO_5$ materials[12], the substituted $BaGd_{2-x}Ca_xCoO_5$ samples from this work present a rather significant fraction of oxidized transition metal cations, with expected positive impact on the electronic transport, as it can be seen in Fig. 5. Based on the previously proposed defect models for Haldane gap nickelates[12,38], the corresponding defect chemistry reactions in this case can be described using the standard Kröger-Vink notation[39] as:

$$BaO + (2-x)GdO_{1.5} + \alpha CaO + CoO \rightarrow Ba_{Ba}^{\times} + \alpha Ca_{Gd}^{'} + (2-x)Gd_{Gd}^{\times} + \beta Co_{Co}^{\bullet} +$$

$$+(1-\beta)Co_{Co}^{\times} + \frac{x-\beta}{2}V_O^{\bullet\bullet} + (5-x-\frac{\beta}{2})O_O^{\times} + \frac{x+\beta}{4}O_2(g) \quad (2)$$

where β represents the contribution provided by the formation of charge carriers Co^{3+} ($Co_{Co}^{\bullet}$). Even minor substitutions (x=0.05) with Ca^{2+} in $BaGd_{2-x}Ca_xCoO_5$ result in a dramatic increase of $[Co^{3+}]/[Co]_{tot}$ fraction, which further decreases for x=0.10-0.20. This decrease is likely contributed by the predominant charge compensation by oxygen vacancies and, for higher cobalt contents, by the exsolution of phase impurities (Fig. 4). This is also suggested by the higher variation of Co^{3+} content with temperature, observed for the compositions with x≥0.10.

In general, these results indicate that the concentration of electronic charge carriers from the prepared compositions is dramatically affected only at relatively low acceptor contents.

3.2. Thermoelectric performance

The electrical conductivity of $BaGd_{2-x}Ca_xCoO_5$ (x=0.00–0.20) samples was evaluated in the temperature range 570-1175 K, under both Ar and air atmospheres (Fig. 6). A typical semiconducting behavior is found for all measured samples, in the whole measured temperature range. 3-10 times enhanced conductivities as compared to the

pristine BGCC0 is observed for calcium-substituted samples, as shown in Fig. 6, in agreement with the calculated density values and the predictions based on the changes of charge carrier concentrations, estimated from TGA studies (Fig. 5).

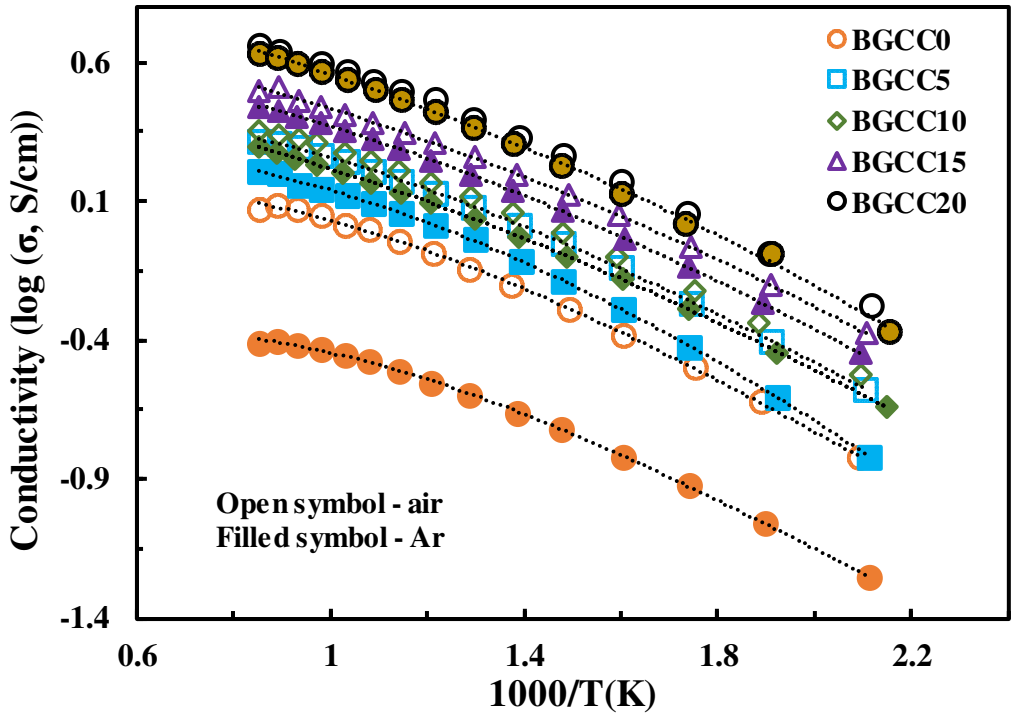

Figure 6. Electrical conductivity values of $BaGd_{2-x}Ca_xCoO_5$ (x=0.00–0.20) samples as a function of temperature, under both Ar and air atmospheres.

Even higher electrical conductivity is observed for the samples measured in air, as compared to the measurements performed in Ar. In this case, oxygen effectively acts as an electronic acceptor, filling the oxygen vacancies and increasing the concentration of Co^{3+} species, combined with similar effects provided by the calcium substitution. This can be described by the following defects reaction:

$$2\,Co_{Co}^{\times} + \frac{1}{2}O_2(g) + V_O^{\bullet\bullet} \rightarrow 2Co_{Co}^{\bullet} + O_O^{\times} \qquad (3)$$

It is worth noticing that under air, the pristine BGCC0 samples show ~3 times higher conductivity as compared to the measurements in Ar. However, the difference in conductivity values measured in Ar and air drastically decreases for Ca-substituted

samples, being noticeable for BGCC5 and further vanishing for higher calcium contents. This fact might be related to the progressive formation of phase impurities on oxidation of the samples with relatively high calcium contents. Although the electrical conductivity studies were performed in agreement with the equilibration criteria described in the Experimental section, further studies are needed to better address the stability issues and redox tolerance of the $BaGd_{2-x}Ca_xCoO_5$ Haldane gap ceramics under air atmosphere.

In both Ar- and air-measured series, the electrical conductivity increases on the substitution with calcium. This cannot be explained by the tendencies observed for the compositional dependence of the charge carrier concentration (Fig. 5) and is most probably associated with changes in carrier mobility[12]. The activation energy values were found to be in the range ~0.18-0.2 eV for all samples, in the temperature range 570-1175 K (Table 3).

Table 3. Activation energy (Ea) of $BaGd_{2-x}Ca_xCoO_5$ (x=0.00–0.20) samples in the temperature range 570-1175 K.

Composition	**Activation energy, Ea (eV)**	
	Ar	**Air**
BGCC0	0.187 ± 0.003	0.200 ± 0.003
BGCC5	0.208 ± 0.003	0.198 ± 0.002
BGCC10	0.198 ± 0.001	0.198 ± 0.001
BGCC15	0.199± 0.001	0.196 ± 0.002
BGCC20	0.208± 0.001	0.203 ± 0.002

The low activation energy values calculated for these materials confirm the thermally induced/activated polaron-hopping-type conduction mechanism, characteristic for these

Haldane gap materials. A similar trend was observed previously by Nasani et al. in BaY_2NiO_5[38] and $BaGd_2NiO_5$[12] materials.

The variation of the Seebeck coefficient values with temperature is presented in Fig. 7, also under air and Ar atmospheres.

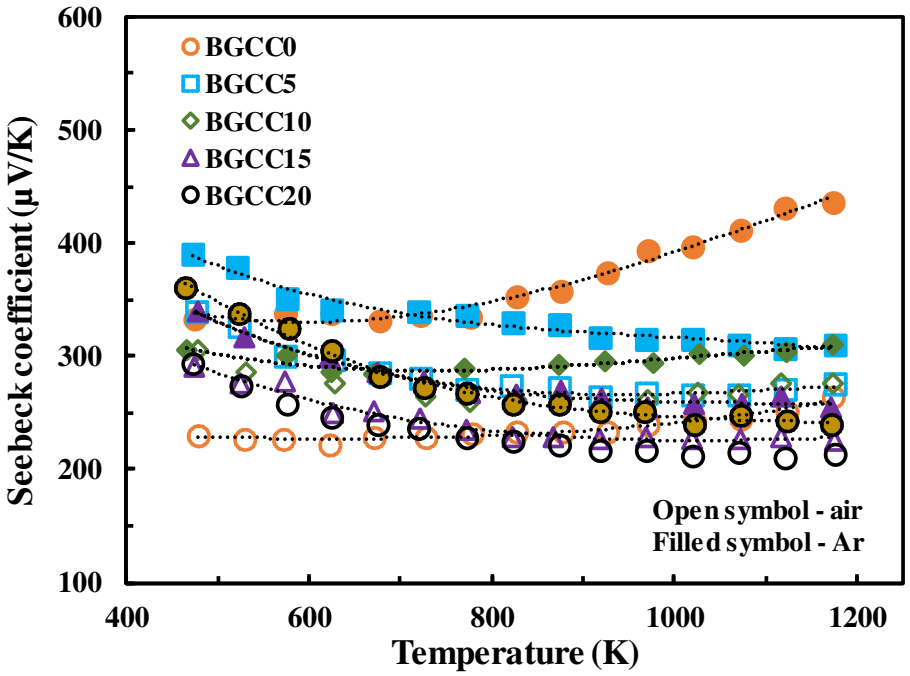

Figure 7. Seebeck coefficient values of $BaGd_{2-x}Ca_xCoO_5$ (x=0.00–0.20) samples as a function of temperature, under both Ar and air atmospheres.

All samples show positive Seebeck coefficient values in the whole measured temperature range, again confirming a p-type semiconducting behavior, with holes being the predominant type of electronic defects, as suggested by the defect chemistry reactions (Eq. 2). The highest Seebeck coefficient value of ~435 μV/K at 1173 K is found for pristine BGCC0 under Ar atmosphere. In contrast, the same sample shows the value of ~264 μV/K at 1173K under air, again confirming the progressive generation of charge carriers which decrease the thermopower value. In general, the observed tendencies agree with the electrical conductivity behavior, namely, the samples with

higher conductivity values show lower Seebeck coefficient, and vice-versa. However, additional insights on charge carrier mobility issues discussed earlier can be obtained from surprisingly low Seebeck coefficient values measured for pristine BGCC0 samples, measured in air, as compared to the substituted samples. This decrease is obviously related to the massive charge carrier generation on oxidation, as revealed by the corresponding ~3 times conductivity increase (Fig. 6). While the amount of these charge carriers is enough to suppress the Seebeck coefficient to one of the lowest measured values, the conductivity of BGCC0 in air is still below the rest of the samples, suggesting the lowest mobility. This hypothesis also agrees with the increase in charge carrier mobility, observed for $BaGd_{2-x}Ca_xNiO_5$ materials, upon substitution with calcium [12].

Fig. 8 represents the cumulative effect of the electrical conductivity and Seebeck coefficient on the thermoelectric performance, expressed as a variation of the power factor ($P=S^2.\sigma$) with temperature under air and Ar atmospheres.

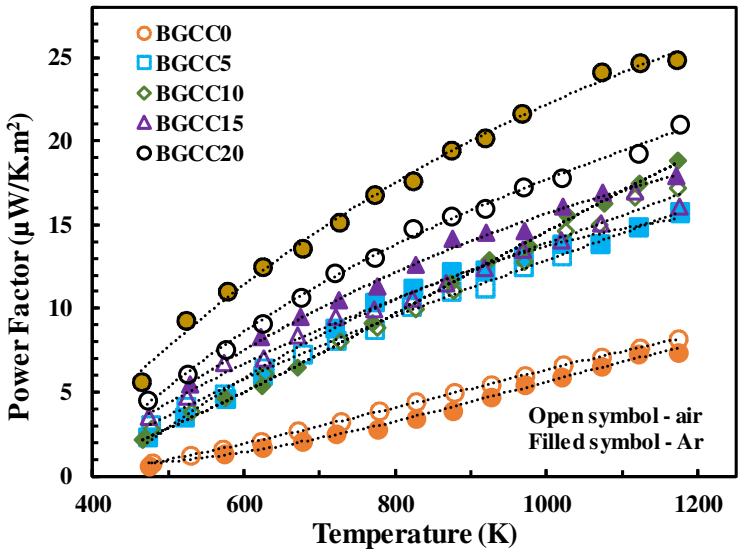

Figure 8. Power factor values of $BaGd_{2-x}Ca_xCoO_5$ (x=0.00–0.20) samples as a function of temperature, under both Ar and air atmospheres.

The power factor is improved by increasing the temperature and Ca substitution. The BGCC20 sample shows the highest power factor value of ~25 μW/K.m^2 at 1173 K, due to the highest electrical conductivity values from the whole range of studied compositions. It should be noticed that these power factor values are notably below those found/measured for state-of-the-art $Ca_3Co_4O_9$ and $SrTiO_3$ thermoelectric oxides. The highest power factor value measured for the $BaGd_2NiO_5$ Haldane gap material is ~21 μW/K.m^2 at 1179 K, as previously reported by our group [12]. Thus, in this context, only a marginal enhancement in power factor values is achieved for calcium substituted $BaGd_2CoO_5$ compositions.

Fig. 9(a) illustrates the variation of total thermal conductivity with temperature, between 400-1200 K. Only a marginal difference (except for BGCC0) between the samples of the same composition measured in Ar and air is observed, suggesting that oxygen vacancies, if any, are only slightly affecting the thermal transport.

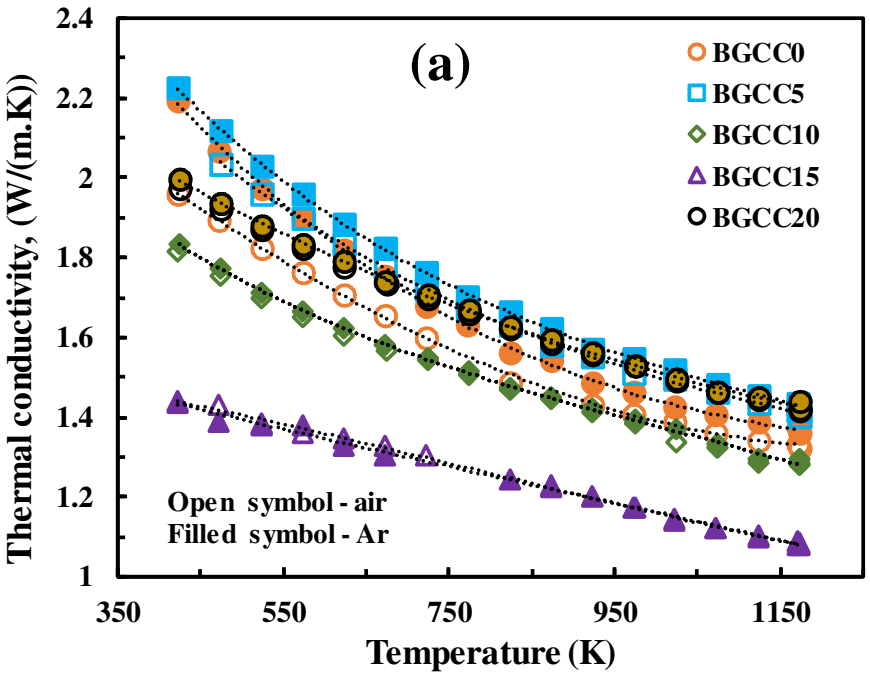

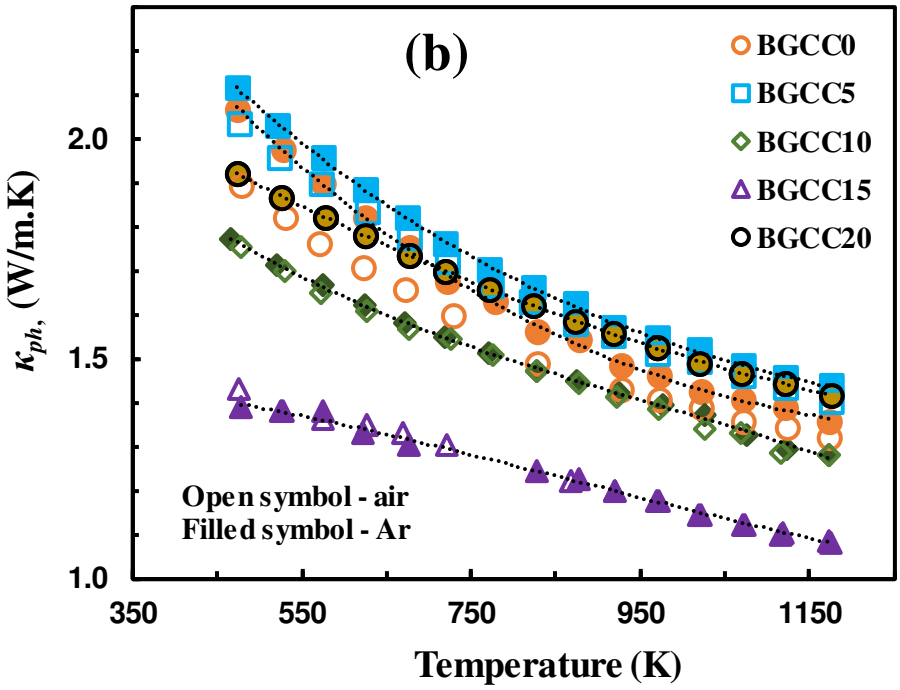

Figure 9. Total thermal conductivity (a) and lattice thermal conductivity (b) values of $BaGd_{2-x}Ca_xCoO_5$ (x=0.00–0.20) samples as a function of temperature, under both Ar and air atmospheres.

In the studied materials, the heat is predominantly transported by phonons, and the contribution of the electronic counterpart does not exceed 1%. Corresponding data for lattice thermal conductivity measurements are shown in Fig. 9(b), where the tendencies observed are essentially similar to those found for the total thermal conductivity (Fig. 9(a)). Therefore, the impact of possible oxygen vacancies on the phonon scattering is apparently negligible, as compared to more pronounced effects observed for strontium titanate-based thermoelectrics[22,24,26,40,41]. This fact most probably stems from the highly anisotropic crystal structure of the Haldane gap materials, which provides rather efficient scattering of phonons, compared to oxygen vacancies, and possibly, to some other type of point defects. The difference between the low thermal conductivity values observed for $BaGd_{2-x}Ca_xCoO_5$ materials and the typical ones found for donor-substituted strontium titanates, also justify this assumption. The thermal conductivity values exhibit an increase from pristine BGCC0 to BGCC5; the reasons for this

behavior being not so well understood. Typically, the generation of point defects by cation substitutions suppresses the thermal transport[42]. A possible explanation for this fact might be based on an intimate interplay between low calcium contents (and, hence, relatively low concentration of point defects) and decrease in unit cell volume (Fig. 2), favorable for higher thermal conductivity values[42]. Upon further increase of the calcium content up to x=0.15, the thermal conductivity drastically decreases and reaches very attractive values, between 1.0-1.4 W/(m.K). It should be noticed that this minimum observed for the BGCC15 samples is also in line with structural and microstructural results, which indicated the solid solution limit corresponding to this composition. Further promotion of microscale-size (Fig. 4) phase impurities shifts the chemical composition of the main phase and decreases the advantage of its anisotropy, resulting in the higher thermal conductivity values measured for the BGCC20 samples. Nevertheless, the thermal conductivity values from this work are among the lowest found in oxides, as illustrated in Table 4.

Table 4. Comparison of the thermal conductivity results from this work with literature data.

Material	**Thermal conductivity (W/m.K)**	**Temperature (K)**	**Reference**
$BaGd_{1.85}Ca_{0.15}CoO_5$	1.08 – 1.44	1173-422	This work
$BaGd_{1.85}Ca_{0.15}NiO_5$	1.59 – 2.15	1179-446	[12]
$BaGd_{1.75}Ca_{0.25}NiO_5$	1.28 – 1.31	1179-446	[12]
Al-doped ZnO nanocomposite	1.8	1000	[43]
$Zn_{0.993}Al_{0.007}O$	9.4	820	[35]
$CaMn_{0.95}Nb_{0.05}O_3$	~1	1000	[13]
Sr_2TiMoO_6	~6	1000	[23]
$SrTi_{0.70}Ta_{0.30}O_{3\pm\delta}$	~2	1000	[44]
$SrTi_{0.85}Nb_{0.15}O_3$ $YSZ/SrTi_{0.85}Nb_{0.15}O_3$	~3 ~2.6	900	[45]

Finally, the temperature dependence of the dimensionless figure-of-merit for all samples is plotted in Fig. 10, between around 450 and 1200 K.

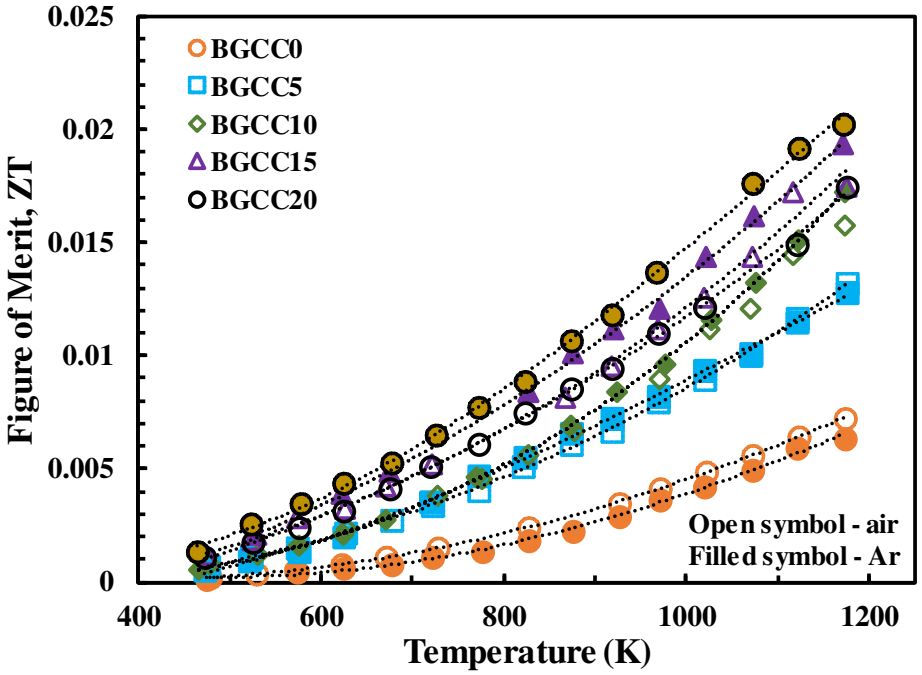

Figure 10. Dimensionless figure of merit values of $BaGd_{2-x}Ca_xCoO_5$ (x=0.00–0.20) samples as a function of temperature, under both Ar and air atmospheres.

The *ZT* values increase with temperature and calcium substitution, reaching the maximum value of ~0.02 for both BGCC15 and BGCC20 at 1173 K. Despite showing the lowest thermal conductivity values among selected oxide-based thermoelectric materials, the thermoelectric efficiency of the materials studied in this work is still below that acceptable for most thermoelectric applications. The underlying reason for this is mainly low electrical conductivity, which can be possibly improved by exploring further possibilities to design acceptor-(co)substituted Haldane gap oxides.

4. Conclusions

In this work, the structural, microstructural, electrical and thermal properties of calcium-substituted $BaGd_2CoO_5$ Haldane gap family materials were studied, to assess these

materials as potential thermoelectrics to operate in inert and air atmospheres and in the relevant temperature range. When using a conventional solid-state synthesis route, followed by sintering at 1553 K for 6 h in argon atmosphere, the solubility limit of calcium allowing the formation of single-phase $BaGd_{2-x}Ca_xCoO_5$ solid solutions with an orthorhombic structure, corresponds to $x \leq 0.15$. The microstructural studies confirmed the formation of highly-dense ceramics and revealed the presence of local calcium- and cobalt-rich impurity phases for $x > 0.15$, which were not detected by XRD, probably because of their small amounts. The substitution with Ca resulted in a significant increase in p-type electronic charge carriers concentration up to the solubility limit, followed by a gradual decrease after that point. The electrical conductivity trends of the prepared ceramic samples, in Ar and air, showed a semiconducting-like behavior and varied in the range 0.06-4.7 S/cm at 570-1175 K. The Seebeck coefficient values were found to lie in the range 210-440 μV/K. The difference in electrical behavior under inert and oxidizing conditions was found to decrease on increasing calcium content. The acceptor-type substitution resulted in a general increase in electrical conductivity, contributed by an intimate interplay between the charge carrier concentration and their mobility. The highest power factor value was for the $BaGd_{1.80}Ca_{0.20}CoO_5$ samples, amounting to ~25 $\mu W/K.m^2$ at 1173 K. The materials from this study demonstrated very low thermal conductivity values, reaching 1.08 W/m.K for $BaGd_{1.85}Ca_{0.15}CoO_5$ at 1173 K, due to the highly-anisotropic structure of the Haldane gap phase, combined with the generation of point defects upon Ca substitutions. The highest dimensionless figure-of-merit of ~0.02 at 1173 K was achieved for the $BaGd_{1.85}Ca_{0.15}CoO_5$ and $BaGd_{1.80}Ca_{0.20}CoO_5$ compositions.

Acknowledgements

N. Nasani acknowledges funding from DST under Inspire faculty program (DST/INSPIRE/04/2017/003334) and C-MET, MeitY, Govt. of India. D. P. Fagg acknowledges FCT Investigator Programme IF/01344/2014/CP1222/CT0001 and Projects PTDC/CTM-ENE/6319/2014, POCI-01-0145-FEDER-032241, UID/EMS/00481/2019-FCT, CENTRO-01-0145-FEDER-022083 - QREN, FEDER and COMPETE Portugal and EU for the financial support. A. Kovalevsky, S. Rasekh and G. Constantinescu acknowledge the support of the project POCI-01-0145-FEDER-031875, financed by COMPETE 2020 Program and National Funds through the FCT/MEC and, when applicable, co-financed by FEDER under the PT2020 Partnership Agreement, and the support of the FCT–CEECIND/02608/2017 grant. This work was partially developed within the scope of the project CICECO-Aveiro Institute of Materials, UIDB/50011/2020 & UIDP/50011/2020, financed by national funds through the FCT/MCTES. W. Xie and A. Weidenkaff would like to acknowledge the financial support from Deutsche Forschungsgemeinschaft (Project No. BA 4171/4-1).

5. References

(1) Tomeš, P.; Trottmann, M.; Suter, C.; Aguirre, M. H.; Steinfeld, A.; Haueter, P.; Weidenkaff, A. Thermoelectric Oxide Modules (TOMs) for the Direct Conversion of Simulated Solar Radiation into Electrical Energy. *Materials (Basel).* **2010**, *3* (4), 2801–2814. https://doi.org/10.3390/ma3042801.

(2) Robert, R.; Bocher, L.; Sipos, B.; Döbeli, M. Ni-Doped Cobaltates as Potential Materials for High Temperature Solar Thermoelectric Converters. *Prog. Solid State Chem.* **2007**, *35* (2–4), 447–455. https://doi.org/10.1016/J.PROGSOLIDSTCHEM.2007.01.020.

(3) Suter, C.; Tomeš, P.; Weidenkaff, A.; Steinfeld, A. Heat Transfer and Geometrical Analysis of Thermoelectric Converters Driven by Concentrated Solar Radiation. *Materials (Basel).* **2010**, *3* (4), 2735–2752. https://doi.org/10.3390/ma3042735.

(4) Freer, R.; Powell, A. V. Realising the Potential of Thermoelectric Technology: A Roadmap. *J. Mater. Chem. C* **2020**, *8* (2), 441–463. https://doi.org/10.1039/c9tc05710b.

(5) Tritt, T. M.; Subramanian, M. A. Thermoelectric Materials, Phenomena, and Applications: A Bird's Eye View. *MRS Bull.* **2006**, *31* (03), 188–198. https://doi.org/10.1557/mrs2006.44.

(6) Zhang, X.; Zhao, L.-D. Thermoelectric Materials: Energy Conversion between Heat and Electricity. *J. Mater.* **2015**, *1* (2), 92–105. https://doi.org/10.1016/j.jmat.2015.01.001.

(7) Weidenkaff, A. Thermoelectrics: Better Half Found. *Nat. Energy* **2017**, *2* (2), 17010. https://doi.org/10.1038/nenergy.2017.10.

(8) Liu, W.; Jie, Q.; Kim, H. S.; Ren, Z. Current Progress and Future Challenges in Thermoelectric Power Generation: From Materials to Devices. *Acta Mater.* **2015**, *87*, 357–376. https://doi.org/10.1016/J.ACTAMAT.2014.12.042.

(9) Bux, S. K.; Fleurial, J. P.; Kaner, R. B. Nanostructured Materials for Thermoelectric Applications. *Chem. Commun.* **2010**, *46* (44), 8311–8324. https://doi.org/10.1039/c0cc02627a.

(10) Ren, G.; Lan, J.; Zeng, C.; Liu, Y.; Zhan, B.; Butt, S.; Lin, Y. H.; Nan, C. W. High Performance Oxides-Based Thermoelectric Materials. *Jom* **2015**, *67* (1), 211–221. https://doi.org/10.1007/s11837-014-1218-2.

(11) Yin, Y.; Tudu, B.; Tiwari, A. Recent Advances in Oxide Thermoelectric Materials and Modules. *Vacuum* **2017**, *146*, 356–374. https://doi.org/10.1016/j.vacuum.2017.04.015.

(12) Nasani, N.; Oliveira Rocha, C. M.; Kovalevsky, A. V.; Otero Irurueta, G.; Populoh, S.; Thiel, P.; Weidenkaff, A.; Neto Da Silva, F.; Fagg, D. P. Exploring the Thermoelectric Performance of BaGd2NiO5 Haldane Gap Materials. *Inorg. Chem.* **2017**, *56* (4). https://doi.org/10.1021/acs.inorgchem.7b00049.

(13) Bocher, L.; Aguirre, M. H.; Logvinovich, D.; Shkabko, A.; Robert, R.; Trottmann, M.; Weidenkaff, A. CaMn1-x NbxO3 ($x \leq 0.08$) Perovskite-Type Phases as Promising New High-Temperature n-Type Thermoelectric Materials. *Inorg. Chem.* **2008**, *47* (18), 8077–8085. https://doi.org/10.1021/ic800463s.

(14) Kovalevsky, A. V. V; Yaremchenko, A. A. A.; Populoh, S.; Thiel, P.; Fagg, D. P. P.; Weidenkaff, A.; Frade, J. R. R. Towards a High Thermoelectric Performance in Rare-Earth Substituted SrTiO3: Effects Provided by Strongly-Reducing Sintering Conditions. *Phys. Chem. Chem. Phys.* **2014**, *16* (48), 26946–26954. https://doi.org/10.1039/c4cp04127e.

(15) Ferreira, N. M.; Ferro, M. C.; Sarabando, A. R.; Ribeiro, A.; Davarpanah, A.; Amaral, V.; Madre, M. A.; Kovalevsky, A. V.; Torres, M. A.; Costa, F. M.; et al. Improvement of Thermoelectric Properties of Ca0.9Gd0.1MnO3 by Powder Engineering through K2CO3 Additions. *J. Mater. Sci.* **2019**, *54* (4), 3252–3261. https://doi.org/10.1007/s10853-018-3058-x.

(16) Ren, G.-K.; Lan, J.-L.; Zhao, L.-D.; Liu, C.; Yuan, H.; Shi, Y.; Zhou, Z.; Lin, Y.-H. Layered Oxygen-Containing Thermoelectric Materials: Mechanisms, Strategies, and Beyond. *Mater. Today* **2019**, *xxx* (xx), 1–18. https://doi.org/10.1016/j.mattod.2019.07.003.

(17) Torres, M. A.; Costa, F. M.; Flahaut, D.; Touati, K.; Rasekh, S.; Ferreira, N. M.;

Allouche, J.; Depriester, M.; Madre, M. A.; Kovalevsky, A. V.; et al. Significant Enhancement of the Thermoelectric Performance in Ca3Co4O9 Thermoelectric Materials through Combined Strontium Substitution and Hot-Pressing Process. *J. Eur. Ceram. Soc.* **2019**, *39* (4), 1186–1192. https://doi.org/10.1016/j.jeurceramsoc.2018.12.049.

(18) Terasaki, I.; Sasago, Y.; Uchinokura, K. Large Thermoelectric Power in NaCo2O4 Single Crystals. *Phys. Rev. B* **1997**, *56* (20), R12685–R12687. https://doi.org/10.1103/PhysRevB.56.R12685.

(19) Tsubota, T.; Ohtaki, M.; Eguchi, K.; Arai, H. Thermoelectric Properties of Al-Doped ZnO as a Promising Oxide Material for High-Temperature Thermoelectric Conversion. *J. Mater. Chem.* **1997**, *7* (1), 85–90. https://doi.org/10.1039/a602506d.

(20) Koumoto, K.; Wang, Y.; Zhang, R.; Kosuga, A.; Funahashi, R. Oxide Thermoelectric Materials: A Nanostructuring Approach. *Annu. Rev. Mater. Res.* **2010**, *40* (1), 363–394. https://doi.org/10.1146/annurev-matsci-070909-104521.

(21) Azough, F.; Gholinia, A.; Alvarez-Ruiz, D. T.; Duran, E.; Kepaptsoglou, D. M.; Eggeman, A. S.; Ramasse, Q. M.; Freer, R. Self-Nanostructuring in SrTiO3: A Novel Strategy for Enhancement of Thermoelectric Response in Oxides. *ACS Appl. Mater. Interfaces* **2019**, *11* (36), 32833–32843. https://doi.org/10.1021/acsami.9b06483.

(22) Kovalevsky, A. V. Defects Engineering for Performing Srtio3-Based Thermoelectric Thin Films: Principles and Selected Approaches. In *Advanced Ceramic and Metallic Coating and Thin Film Materials for Energy and Environmental Applications*; Springer International Publishing: Cham, 2017; pp 91–120. https://doi.org/10.1007/978-3-319-59906-9_4.

(23) Saxena, M.; Maiti, T. Effect of Ba-Doping on High Temperature Thermoelectric Properties of Sr2TiMoO6 Double Perovskites. *J. Alloys Compd.* **2017**, *710*, 472–478. https://doi.org/10.1016/j.jallcom.2017.03.264.

(24) Kovalevsky, A. A. V.; Aguirre, M. H. M. H.; Populoh, S.; Patrício, S. G. S. G.; Ferreira, N. M. N. M.; Mikhalev, S. M. S. M. S. M.; Fagg, D. P. duncan paul; Weidenkaff, A.; Frade, J. Designing Strontium Titanate-Based Thermoelectrics: An Insight into Defect Chemistry Mechanisms. *J. Mater. Chem. A* **2017**, *5* (8), 3909–3922. https://doi.org/10.1039/C6TA09860F.

(25) Kovalevsky, A. V.; Populoh, S.; Patrício, S. G.; Thiel, P.; Ferro, M. C.; Fagg, D. P.; Frade, J. R.; Weidenkaff, A. Design of SrTiO3-Based Thermoelectrics by Tungsten Substitution. *J. Phys. Chem. C* **2015**, *119* (9), 4466–4478. https://doi.org/10.1021/jp510743h.

(26) Kovalevsky, A. V. V.; Yaremchenko, A. A. A.; Populoh, S.; Weidenkaff, A.; Frade, J. R. R. Effect of A - Site Cation Deficiency on the Thermoelectric Performance of Donor-Substituted Strontium Titanate. *J. Phys. Chem. C* **2014**, *118* (9), 4596–4606. https://doi.org/10.1021/jp409872e.

(27) Butt, S.; Xu, W.; He, W. Q.; Tan, Q.; Ren, G. K.; Lin, Y.; Nan, C. W. Enhancement of Thermoelectric Performance in Cd-Doped Ca3Co4O9via Spin Entropy, Defect Chemistry and Phonon Scattering. *J. Mater. Chem. A* **2014**, *2*

(45), 19479–19487. https://doi.org/10.1039/c4ta03891f.

(28) Saini, S.; Yaddanapudi, H. S.; Tian, K.; Yin, Y.; Magginetti, D.; Tiwari, A. Terbium Ion Doping in Ca 3 Co 4 O 9: A Step towards High-Performance Thermoelectric Materials. *Sci. Rep.* **2017**, *7* (1), 44621. https://doi.org/10.1038/srep44621.

(29) Ji, L. Metal Oxide-Based Thermoelectric Materials. In *Metal Oxides in Energy Technologies*; Elsevier, 2018; pp 49–72. https://doi.org/10.1016/b978-0-12-811167-3.00003-1.

(30) Hernández-Velasco, J.; Salinas-Sánchez, A.; Sáez-Puche, R. Antiferromagnetic Ordering and Structural Characterization of the Brown Colored R2BaCoO5 Oxides (R = Rare Earth). *J. Solid State Chem.* **1994**, *110* (2), 321–329. https://doi.org/10.1006/jssc.1994.1175.

(31) Wechsel, E.; Oxiden, D.; Muller-buschbaum, H. M. H. K.; Chemie, A. Ein Wechsel Des Strukturtyps in Den Oxiden BaCoGd2O5, BaCoDy2O5 Und BaCoY2O5. **1989**, *573*, 128–132.

(32) Rodríguez-Carvajal, J. Recent Advances in Magnetic Structure Determination by Neutron Powder Diffraction. *Phys. B Condens. Matter* **1993**, *192* (1–2), 55–69. https://doi.org/10.1016/0921-4526(93)90108-I.

(33) Tiflova, L. A.; Kovba, M. L.; Monaenkova, A. S. Thermochemical Properties of Ln2BaCoO5 (Ln = Nd, Gd, Dy, Ho). *Russ. J. Phys. Chem. A* **2015**, *89* (4), 604–607. https://doi.org/10.1134/S003602441504024X.

(34) Kovalevsky, A. V. V.; Yaremchenko, A. A. A.; Populoh, S.; Weidenkaff, A.; Frade, J. R. R. Enhancement of Thermoelectric Performance in Strontium Titanate by Praseodymium Substitution. *J. Appl. Phys.* **2013**, *113* (5), 053704. https://doi.org/10.1063/1.4790307.

(35) Zakharchuk, K. V.; Tobaldi, D. M.; Xiao, X.; Xie, W.; Mikhalev, S. M.; Martins, J. F.; Frade, J. R.; Weidenkaff, A.; Kovalevsky, A. V. Synergistic Effects of Zirconium- and Aluminum Co-Doping on the Thermoelectric Performance of Zinc Oxide. *J. Eur. Ceram. Soc.* **2019**, *39* (4), 1222–1229. https://doi.org/10.1016/j.jeurceramsoc.2018.11.029.

(36) Chester, G. V; Thellung, A. The Law of Wiedemann and Franz. *Proc. Phys. Soc.* **1961**, *77* (5), 1005–1013. https://doi.org/10.1088/0370-1328/77/5/309.

(37) Lannuzel, F.-X.; Janod, E.; Payen, C.; Ouvrard, G.; Moreau, P.; Chauvet, O.; Parent, P.; Laffon, C. Electronic Structure of a Hole Doped Oxide with a Quasi-1D Crystal Structure Y2−x(Sr,Ca)XBaNiO5. *J. Alloys Compd.* **2001**, *317–318*, 149–152. https://doi.org/10.1016/S0925-8388(00)01337-2.

(38) Nasani, N.; Ramasamy, D.; Antunes, I.; Singh, B.; Fagg, D. P. Structural and Electrical Properties of Strontium Substituted Y2BaNiO5. *J. Alloys Compd.* **2015**, *620*, 91–96. https://doi.org/10.1016/j.jallcom.2014.09.127.

(39) Kröger, F. A.; Vink, H. J. Relations between the Concentrations of Imperfections in Crystalline Solids. *Solid State Phys. - Adv. Res. Appl.* **1956**, *3* (C), 307–435. https://doi.org/10.1016/S0081-1947(08)60135-6.

(40) Popuri, S. R.; Decourt, R.; McNulty, J. A.; Pollet, M.; Fortes, A. D.; Morrison, F.

D.; Senn, M. S.; Bos, J. W. G. Phonon-Glass and Heterogeneous Electrical Transport in A-Site-Deficient SrTiO3. *J. Phys. Chem. C* **2019**, *123* (9), 5198–5208. https://doi.org/10.1021/acs.jpcc.8b10520.

(41) Popuri, S. R.; Scott, A. J. M.; Downie, R. A.; Hall, M. A.; Suard, E.; Decourt, R.; Pollet, M.; Bos, J.-W. G. Glass-like Thermal Conductivity in SrTiO 3 Thermoelectrics Induced by A-Site Vacancies. *RSC Adv.* **2014**, *4* (64), 33720–33723. https://doi.org/10.1039/C4RA06871H.

(42) Snyder, G. J.; Toberer, E. S. Complex Thermoelectric Materials. *Nat. Mater.* **2008**, *7* (2), 105–114. https://doi.org/10.1038/nmat2090.

(43) Jood, P.; Mehta, R. J.; Zhang, Y.; Peleckis, G.; Wang, X.; Siegel, R. W.; Borca-Tasciuc, T.; Dou, S. X.; Ramanath, G. Al-Doped Zinc Oxide Nanocomposites with Enhanced Thermoelectric Properties. *Nano Lett.* **2011**, *11* (10), 4337–4342. https://doi.org/10.1021/nl202439h.

(44) Yaremchenko, A. A. A.; Populoh, S.; Patrício, S. G. S. G.; Macías, J.; Thiel, P.; Fagg, D. P. D. P.; Weidenkaff, A.; Frade, J. R.; Kovalevsky, A. V. A. V. Boosting Thermoelectric Performance by Controlled Defect Chemistry Engineering in Ta-Substituted Strontium Titanate. *Chem. Mater.* **2015**, *27* (14), 4995–5006. https://doi.org/10.1021/acs.chemmater.5b01389.

(45) Wang, N.; Chen, H.; He, H.; Norimatsu, W.; Kusunoki, M.; Koumoto, K. Enhanced Thermoelectric Performance of Nb-Doped SrTiO3 by Nano-Inclusion with Low Thermal Conductivity. *Sci. Rep.* **2013**, *3*, 3449. https://doi.org/10.1038/srep03449.

For Table of Contents Only